CrossMark

DTA Determination of Phase Equilibria in the Ternary Ag-Sb-Sn System

Joanna Łapsa[1] · Bogusław Onderka[1]

© The Author(s) 2018

Abstract The experimental data on phase transitions temperatures in Ag-Sb-Sn system have been obtained by DTA technique during heating and cooling cycles. To verify phase equilibria in this system, a number of 19 different samples were studied in the temperature range 100-850 °C. The existence of coexisting phases and their composition was analysed by SEM and EDX techniques for 5 distinct samples after their thermal equilibration at 400 °C. The obtained data were compared with isopleths calculated from available literature assessments.

Keywords isothermal equilibration · metals and alloys · phase diagrams · thermal analysis

1 Introduction

The pressure from EU legislature to prohibit the use of lead containing solders stimulated the search for new, lead-free materials. Two subsequent COST Actions, 531 and MP0602, selected a number of alloys which can be used as a substitute for traditional Pb-Sn solder. One of them, (Ag-Sn alloy) was found to be a suitable material, however

✉ Bogusław Onderka
   onderka@agh.edu.pl

[1] Department of Non-Ferrous Metals, AGH University of Science and Technology, 30 Mickiewicza Avenue, 30-059 Kraków, Poland

additional elements were needed to suppress its coarsening. Lee et al.[1,2] investigated the influence of Sb addition into Sn-matrix on the microstructure, adhesive strength and fatigue of Ag-Sb-Sn alloys working as solder joints. They found that the addition of antimony causes solid solution hardening and depresses the growth of the interfacial intermetallic compound layers. It also improves adhesive strength and thermal resistance of Sn35Ag alloy. The investigation of the influence of Sb content on reliability of SnAgSb solder showed that fatigue life of the joints increases with the amount of Sb added. Consequently, the Ag-Sb-Sn system attracted the attention as the one being chosen for a new lead-free solder material.

Needless to say, phase relations in this system, especially in the concentration range close to binary Ag-Sn eutectic, became an object of great interest. Masson and Kirkpatrick[3] investigated liquidus surface and identified invariant reactions using DTA and microprobe analysis. They presented liquidus projection and determined composition of co-existing phases for the two invariant reactions.

Further studies of phase equilibria in Ag-Sb-Sn system were conducted by Oberndorff et al.,[4] who constructed an isothermal cross-section through the ternary system at 220 °C. They used diffusion couples and analysis of equilibrated alloys. This work showed that SbSn compound is not present in the equilibrium phase at this temperature. They identified also solid solution between intermetallic phases labeled ζ-phase. For the phase notation and structure see Table 1.

In their Materials Science International Team (MSIT) publication (http://www.msiport.com/), Schmid-Fetzer et al.[5] reviewed the existing literature data for constituent binaries and ternary Ag-Sb-Sn.

Table 1 Phases in the Ag-Sb-Sn ternary system[11]

Phase	Strukturbericht designation	Pearson symbol	Prototypes
Liquid	…	…	…
(Ag)	A1	$cF4$	Cu
(Sb)	A7	$hR2$	α-As
βSn	A5	$tI4$	β-Sn
αSn	A4	$cF8$	C (diamond)
SbSn	B1	$cF8$	NaCl
Sb_2Sn_3	…	…	…
ζ-hcp	A3	$hP2$	Mg (hcp)
ε	$L6_0$	$tP4$	Cu_3Ti

More extensive studies on ternary Ag-Sb-Sn phase diagram were conducted almost in the same time by Lin et al.[6] and Lee et al.[7] They investigated isothermal sections of the ternary system at 150, 260 and 400 °C, respectively. These studies confirmed that there is a mutual solid solubility between Ag_3Sn and Ag_3Sb intermetallic phases (ε phase) as well as between Ag_4Sn and Ag_4Sb phases (ζ phase). Equilibrium phases found in this temperature range are very similar to one another. Moreover, Lee et al.[7] investigated also interfacial reactions between Sb-Sn alloy and Ag substrate.

Following previous works Chen et al.[8] determined experimentally an isothermal section at 250 °C and liquidus projection of the ternary Ag-Sb-Sn system. They found three tie-triangles: $L + Sb_2Sn_3 + \varepsilon$, $Sb_2Sn_3 + SbSn + \varepsilon$ and $SbSn + (Sb) + \varepsilon$. They also identified three ternary invariant reactions at 379, 314 and 233 °C, respectively. Chen et al.[8] concluded that ζ-Ag_5Sn and ζ-$Ag_{17}Sb_3$ phases form continuous solid solution.

However, temperatures of these invariant reactions are different from the calculated results by Oh et al.[9] The biggest difference is in four-phase equilibrium $L + SbSn \leftrightarrow Sb_2Sn_3 + \varepsilon$, which differs from $L + \varepsilon + SbSn \leftrightarrow Sb_2Sn_3$ equilibrium suggested by Oh et al.[9] Calculations of Oh et al.[9] were based on the liquidus projection given by Masson and Kirkpatric,[3] who did not report $SbSn/Sb_2Sn_3$ boundary and also did not detect Sb_2Sn_3 phase. It was the beginning of the discrepancy between different visions of this Sn-rich corner of the ternary system, which results from the accepted constitution of Sb-Sn binary system.

In parallel to the studies of experimental surface tension and density of Sn-3.8 at.% Ag eutectic base liquid alloys (with 0.03, 0.06 and 0.09 molar fraction of Sb) at a temperature range from 550 to 1200 K, Moser et al.,[10] performed solidification simulation and analysed the change of the terminating temperatures of solidification process. Moreover, they performed experimental determination of phase diagram and optimization of thermodynamic model

parameters of phases in the Ag-Sb-Sn system by the DSC and thermal equilibration method.

Since the new solder may be located at Sn-rich corner of the system, it was important to resolve this problem due to the uncertainty of the solidification temperature. Consequently, Gierlotka et al.[11] recalculated ternary system and reported three class II ternary invariant reactions: $L + (Sb) \leftrightarrow \varepsilon + SbSn$, $L + SbSn \leftrightarrow Sb_2Sn_3 + \varepsilon$ and $L + Sb_2Sn_3 \leftrightarrow \beta Sn + \varepsilon$, which take place at 379, 313 and 231 °C, respectively. However, the range of the stability of Sn_3Sb_2 phase is still not certain. In their model, the Sn_3Sb_2 phase is stable down to room temperature. They modelled continuous solid solution ζ (hcp_A3) as a substitutional solution.

The problem returned with the study of Li et al.[12] who studied this ternary system calorimetrically and by DSC method to identify the temperature of the invariant reactions and to suggest the reactions scheme. In this work authors claim that Sn_3Sb_2 phase is not stable at low temperature, and they proposed one more invariant reaction $Sb_2Sn_3 \leftrightarrow \varepsilon + SbSn + \beta$-Sn below 211 °C (Table 5).

The problems with the description of the part of low temperature equilibria will be even more difficult, since in their recent paper Schmetterer et al.[13] suggested that Sb_2Sn_3 phase does not exist at all. Instead, there is a Sb_3Sn_4 phase present in the binary Sb-Sn system. However, there is still an open question if this observed phase is an independent compound.

As far as thermodynamic properties of Ag-Sb-Sn liquid solutions are concerned, the situation is much more clear. This system was investigated calorimetrically by Gather et al.[15] and Li et al.[12] Their results agree well at 950 °C across the whole composition range. Recently, Łapsa and Onderka[14] published the paper in which except for the heat of mixing data, activities of tin in liquid phase were reported. They were measured with the e.m.f cell with the solid electrolyte. Papers[12,14,15] provide complete description of the liquid phase in this ternary system.

From the above brief literature survey one can conclude that while the liquid phase has been thoroughly

investigated, the relation between solid phases still can be questioned. Therefore, it was decided to enlarge this kind of information and to conduct further studies of phase relations in this ternary system by using DTA experiments.

2 Experimental

The ternary alloy samples were prepared from pieces of pure elements: Ag (99.99%, Aldrich, USA), Sn (99.99%, POCh, Poland) and Sb (> 99.5%, Fluka AG, Switzerland). After melting in evacuated quartz capsules at 800 °C, all samples were held at 300 °C for 15 days to obtain thermodynamic equilibrium. After equilibration, specimens were quenched in iced water and sealed again under vacuum in self-made quartz crucibles. The total weight of the samples used for the thermal analysis experiments was about 250 mg.

Liquidus temperatures and phase transformation temperatures were determined by differential thermal analysis (DTA), which was carried out in an atmosphere of flowing argon. Samples for DTA investigations were chosen along five cross-sections of the ternary phase diagram: $x_{Sn}/x_{Ag} = 0.4286$, $x_{Sn}/x_{Ag} = 2.333$, $x_{Sn}/x_{Sb} = 2.333$, $x_{Ag}/x_{Sb} = 1$ and $x_{Sn} = 0.2$. The composition of studied 19 samples is shown in Fig. 1. The measurements of selected samples were performed on DTA/DSC (differential scanning calorimetry) 404 F1 Pegasus NETZSCH (Germany) apparatus in the temperature range from 100 to 850 °C. The DTA instrument consists of a single furnace and a
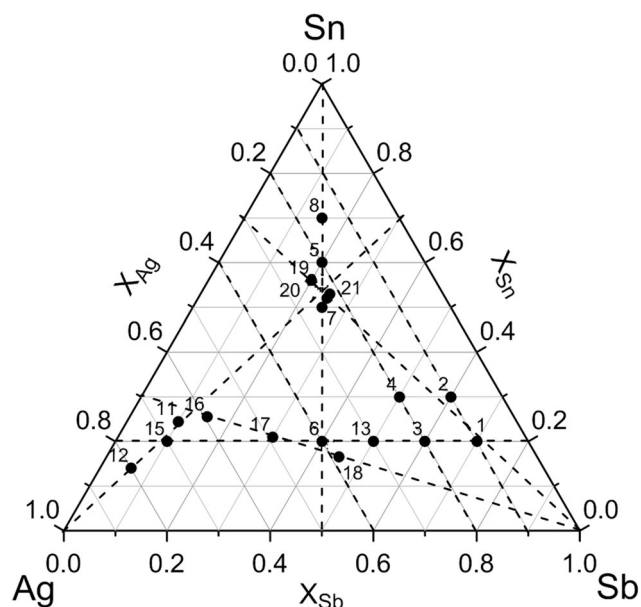
symmetrical sample carrier with positions for the sample and the reference. A sketch of quartz DTA crucible containing the sample is shown in Fig. 2. The empty sealed quartz DTA crucible was adopted as a reference. Calibration was done using the melting points of the high purity metals, In, Sn, Pb, Zn, Al, and Au to establish an internal calibration file. The calibrating samples were also sealed under vacuum in quartz crucibles.

The total experimental error of the method has been estimated to be ± 2 °C. Generally, two heating and cooling cycles were recorded for each sample. The minimum temperature between the cycles was 60 °C in order to allow for possible supercooling. The heating/cooling rate was 5 °/min for both cycles. Additionally, to check the reliability of this rate, the DTA curves at 1 and 10 °/min were recorded for some samples. Liquidus temperatures on heating were evaluated from the peak maximum while those on cooling from the corresponding endset. An example of DTA heating cycles at 1, 5 and 10 °/min scanning rate is shown in Fig. 3. Although it was demonstrated by Boettinger et al.[16] that for multi-component alloys the peak maximum may (depending on a number of parameters, including the heating rate) yield temperature values somewhat higher than the true liquidus temperature, this evaluation is still considered a very good approximation, especially with heating rates of 5 °/min or less. The heating rate of 1 °/min allows to separate the signal features as is shown in Fig. 3 in temperature range from 300 to 350 °C.

Besides thermal analysis, isothermal equilibration studies were also conducted. After sealing samples under vacuum, ternary alloys after pre-melting at 800 °C were kept at constant temperature 400 °C for 30 days, and at 300 °C for 60 days. After quenching in iced water they
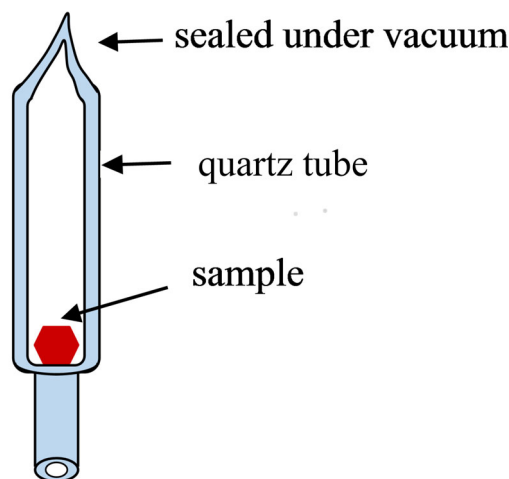

Fig. 1 The compositions of studied samples

Fig. 2 A sketch of the self-made quartz DTA crucible

56

J. Phase Equilib. Diffus. (2019) 40:53–63

were examined by metallographic and Electron Probe Microanalysis (EPMA) analysis. For quantitative EPMA results, the samples were analysed using an acceleration voltage of 20 kV with cobalt as calibration standard for the beam current, gain and resolution of the spectrometer. The x-ray intensities were corrected for Z Absorption Fluorescence (ZAF) effects using pure elements as standards. Microanalysis (EPMA) was used to check the overall composition of the samples, the uniformity of chemical composition, and the composition of the coexisting phases.

3 Results

Subsequent Fig. 4, 5, 6, and 7 show results obtained from DTA measurements for the total of 19 samples located in the respective four cross-sections (isopleths) investigated in this study. The experimental results are also collected in Tables 2, 3 and 4 together with the initial compositions. The coherence with other thermal analysis data were observed, especially, comparing our own data with the results of calculation of: Oh et al.[9]—Fig. 4 and 6 and Gierlotka et al.[11]—Fig. 5 and 7. In the terminal left figure the phase fields were described for the phase diagram calculated from parameters assessed by Moser et al.[10]

Fig. 3 Example of DTA heating cycles at 1, 5 and 10 °/min scanning rate of sample s.5 of composition $Ag_{0.2}Sb_{0.2}Sn_{0.6}$
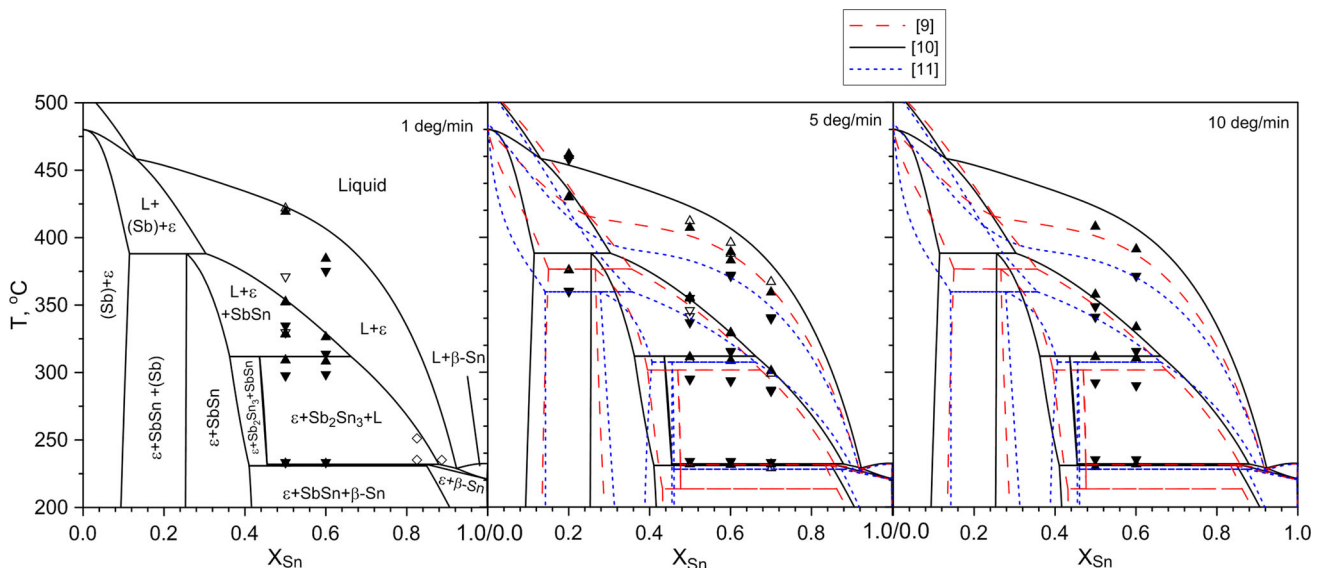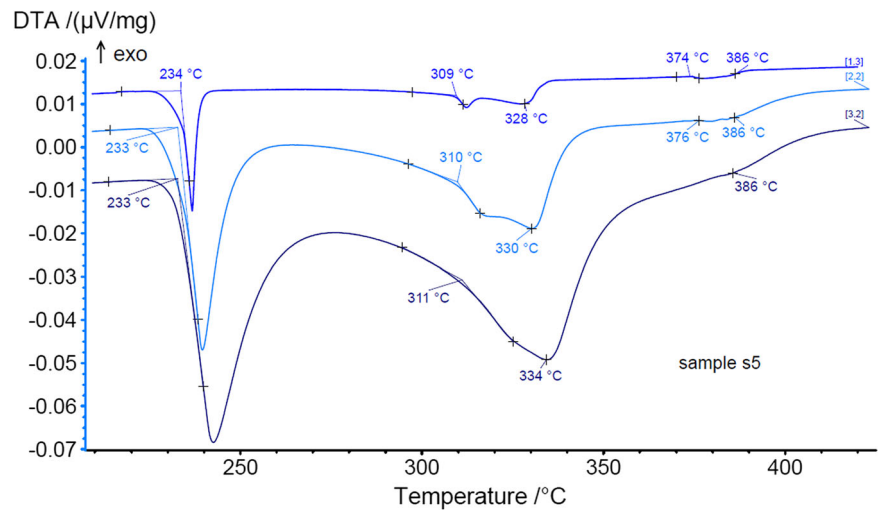

Fig. 4 Experimental data compared with calculated for the x_{Ag}/x_{Sb} = 1 section of Ag-Sb-Sn system of Ref 9-11. The data of Masson et al.[3] were superimposed: diamond symbols description: filled triangle—h1, open triangle—h2, inverted filled triangle—c1, inverted open triangle—c2 (Tables 2, 3, and 4)

Fig. 5 Experimental data compared with calculated for the section $x_{Sn} = 0.2$ of Ag-Sb-Sn system from assessments.[9-11] The experimental data of Moser et al.[10] were superimposed: diamond symbols description: filled triangle—h1, open triangle—h2, inverted filled triangle—c1, inverted open triangle—c2 (Tables 2, 3, and 4)
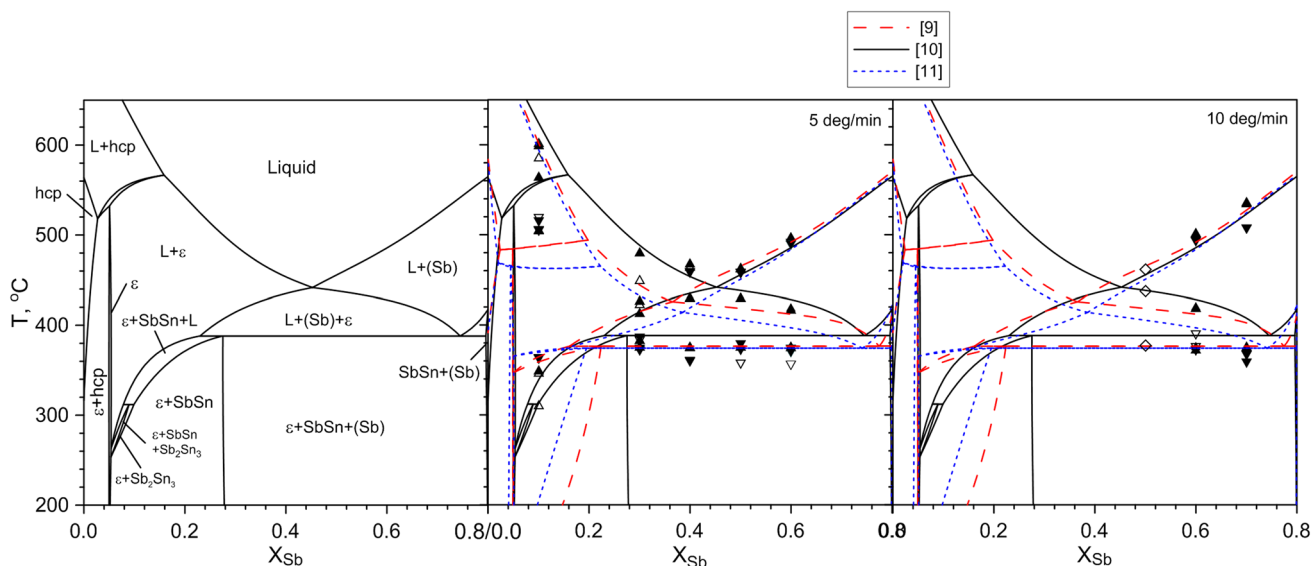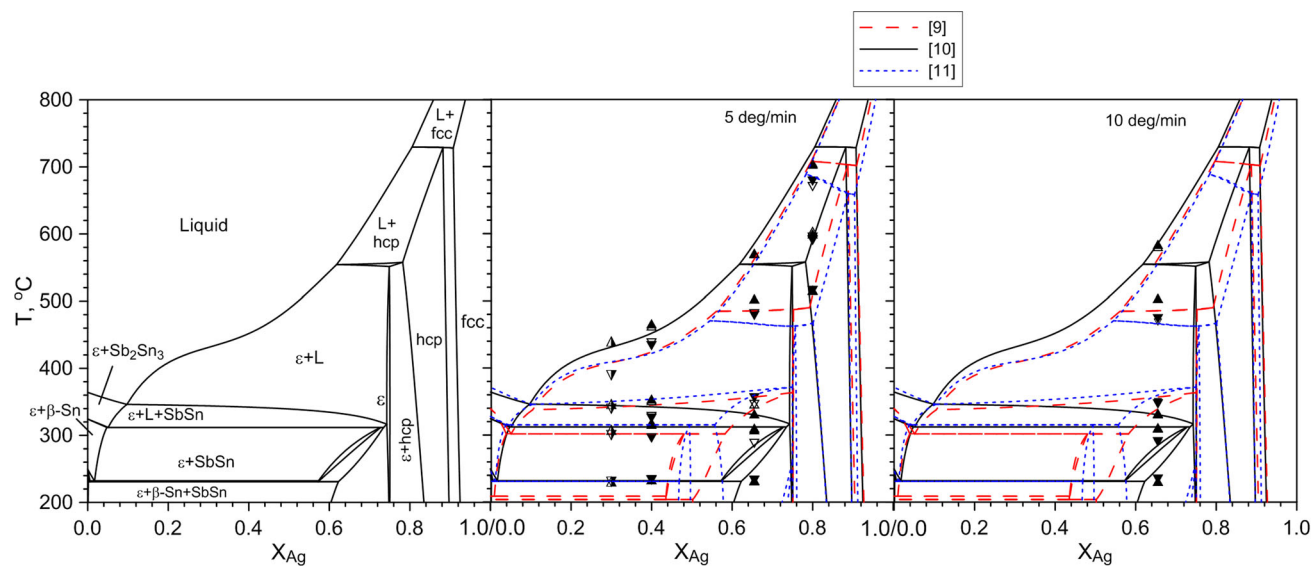

Fig. 6 Experimental data compared with the Ag-Sb-Sn system section at $x_{Sn}/x_{Sb} = 2.333$ calculated from Ref 9-11. The experimental data of Li et al.[12] detected at 1 °/min were superimposed: partial open filled triangle—heating and partial inverted open filled triangle—cooling. Symbols description: filled triangle—h1, open triangle—h2, inverted filled triangle—c1, inverted open triangle—c2 (Tables 2, 3, and 4)

(black solid line). For diagram clarity in this phase diagram other assessments were not enclosed.

For all samples of compositions located in Sn rich range the detected temperature of liquidus is close to the liquidus surface calculated from Oh's assessment[9] regardless of the heating rate (Fig. 4).

The temperature of U₃ reaction obtained in this work agrees in the range of experimental error with other

experimental data as well as with the results of model calculations[9-11] (Fig. 4 and 6).

The same conclusion can be drawn for the temperature of reaction U₂, but the significant undercooling was observed during cooling cycles (Fig. 4 and 5). While the experimental temperature of reaction U₁ is similar to that calculated from assessments of Oh et al.[9] and Gierlotka et al.,[11] it differs more than 3% from the calculated value of Moser et al.[10] (Fig. 4, 5 and 7).
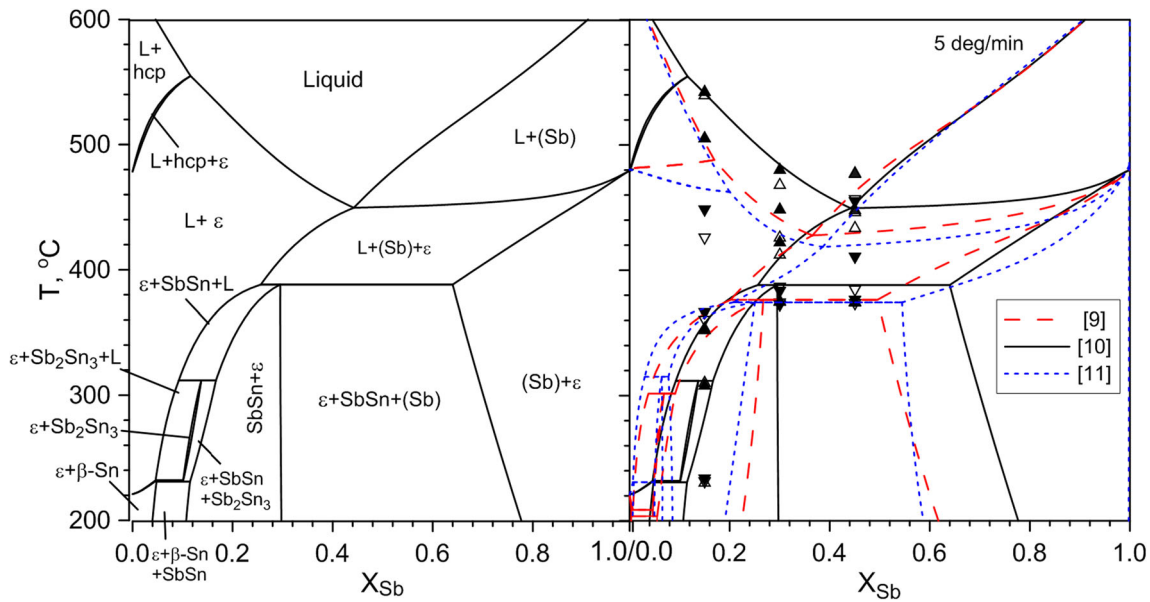
Fig. 7 DTA data obtained in present work shown on the Ag-Sb-Sn system section at $x_{Sn}/x_{Ag} = 0.4286$ calculated from Ref 9-11. Symbols description: filled triangle—h1, open triangle—h2, inverted filled triangle—c1, inverted open triangle—c2 (Tables 2, 3, and 4)

Figure 5 shows that antimony-rich liquidus for $x_{Sn} = 0.2$ diagram section is consistent with all assessments.[9-11] In turn, in case of $x_{Sn}/x_{Ag} = 0.4286$ section, the liquidus temperatures (Table 2) agree well with calculated data of Moser et al.[10] (Fig. 7).

The difference of 2°-3° can be observed between DTA results obtained for invariant reactions at the rate 10 °/min for sample s11 ($Ag_{0.65}Sb_{0.105}Sn_{0.245}$) and sample (55) (Sn-30 at. pct, Sb-10 at. pct, Ag)[8]: 230.9/233.0 and 310.9/314.0, respectively. It should be noted that in the paper of Chen et al.,[8] for all reactions the temperatures were determined from peaks not from the onset which can generate overestimation of the temperature of invariant reactions.

Similarly, comparing DTA results for invariant reaction at the rate 1 °/min obtained for samples s1-2 ($Ag_{0.1}Sb_{0.7-}Sn_{0.2}$ and $Ag_{0.1}Sb_{0.6}Sn_{0.3}$) and sample (13) (Sn-15 at. pct, Sb-684 at. pct, Ag)[3] (1.5 °/min), the difference of 2.5° can be observed: 377 and 379.5 °C, respectively.

A typical DTA curves of one heating cycle obtained with rates 1, 5 and 10 °/min for sample s.5 ($Ag_{0.2}Sb_{0.2-}Sn_{0.6}$) are shown as an example in Fig. 3. It demonstrates that rates lower than standard 10 °/min are more appropriate in the DTA experiments in this system to determine an onset temperature from the thermal signals.

Generally, during cooling cycles performed at the rate 5 °/min, a significant liquidus undercooling of 20-50 °C was observed for almost all samples (Table 2) and even about 100 °C in the samples s.15-17.

The difference of the thermal signals of first and second cycle was observed in some samples (Table 2, s.3, 11, 15,

17, 18) which is the evidence of the retardation of phase precipitation during cooling with 5 °/min rate.

Additionally, the thermal feature of 328-330 °C was detected as a signal peak in 1 °/min rate cycle of samples s.5 and s. 7. Such result is close to the invariant reaction P1: $L + \varepsilon + SbSn \leftrightarrow Sb_2Sn_3$ at 328.9 °C calculated from the assessment of Oh et al.[9] It seems that the answer of the reactions in the ternary system gives us a construction of reliable binary Sb-Sn phase diagram,[13] especially the analysis of the Sb_2Sn_3 compound stability range.

The comparison of invariant reaction temperatures determined by experimental and assessment methods in Ag-Sb-Sn system is shown in Table 5.

The determination of phase constituents at the end of tie-lines and composition of coexisting phases of 5 samples was done by SEM and EDX techniques after their thermal equilibration at 400 °C during 30 days. The examples of micrographs of equilibrated samples (0.74Ag-0.134Sb-0.126Sn and 0.74Ag-0.082Sb-0.178Sn) are shown in Fig. 8. The initial and final compositions are shown in Table 6. The results obtained in temperature 400 °C are very similar to the results of Lin et al.[6] investigation of the isothermal section of the ternary system at the same temperature. First three samples (1, 2, 3, Table 6) show equilibration results as the one detected in sample (20) 0.1Ag.85Sb0.05Sn of,[6] in which also two-phase equilibrium $\varepsilon + (Sb)$ has been determined (Fig. 8a). The initial composition of equilibrated samples (1-4) was chosen close to the stability limit of ε phase. So at BSE microphotographs in Fig. 8(a) and (b) the precipitation of second

Table 2 Heating and cooling features recorded during two temperature cycles with 5 °/min

Sample composition (sample no.)	Cycle (a)	Thermal signals Heating (b) and cooling (c) features, °C
$Ag_{0.1}Sb_{0.7}Sn_{0.2}$ (s.1)	h1	377 o, 535 p
	h2	377 o, 534 p
	c1	357, 366, 498
	c2	357.3, 365.7, 501
$Ag_{0.2}Sb_{0.6}Sn_{0.2}$ (s.3)	h1	376 o, 418 p, 498 p
	h2	376 o, 418 p, 497 p
	c1	369, 373, 488
	c2	355, 490
$Ag_{0.2}Sb_{0.5}Sn_{0.3}$ (s.4)	h1	357 o, 376 o, 402 p, 462 p
	h2	356 o, 375 o, 400 p, 463 p
	c1	360, 361, 442
	c2	361, 363, 448
$Ag_{0.2}Sb_{0.2}Sn_{0.6}$ (s.5)	h1	233 o, 310 o, 330 p, 376 o, 386 p
	h2	233 o, 310 o, 330 p, 389 p, 397 p
	c1	233, 292, 314, 370
	c2	233, 293, 314, 371
$Ag_{0.4}Sb_{0.4}Sn_{0.2}$ (s.6)	h1	376 o, 431 p, 469 p
	h2	377 o, 431 p, 465 p
	c1	359, 457
	c2	359, 457
$Ag_{0.25}Sb_{0.25}Sn_{0.5}$ (s.7)	h1	233 o, 312 o, 357 p, 408 p
	h2	233 o, 311 o, 356 p, 413 p
	c1	233, 294, 336, 354
	c2	233, 294, 340, 345
$Ag_{0.15}Sb_{0.15}Sn_{0.7}$ (s.8)	h1	233 o, 302 p, 360 p
	h2	230 o, 300 p, 368 o
	c1	232, 286, 339
	c2	232, 285, 400
$Ag_{0.4}Sb_{0.18}Sn_{0.42}$ (s.10)	h1	233 o, 319 p, 354, 466 p
	h2	233 o, 316 p, 351, 462 p
	c1	233, 295, 325, 433
	c2	233, 296, 327, 437
$Ag_{0.65}Sb_{0.105}Sn_{0.245}$ (s.11)	h1	233 o, 308 o, 503 o, 570 p
	h2	232 o, 311 o, 346 o, 503 o, 571 p
	c1	232, 356, 478
	c2	232, 287, 346, 481
$Ag_{0.8}Sb_{0.06}Sn_{0.14}$ (s.12)	h1	515 o, 599 p, 705 p
	h2	516 o, 604 p, 704 p
	c1	515, 590, 678
	c2	515, 594, 700
$Ag_{0.3}Sb_{0.5}Sn_{0.2}$ (s.13)	h1	377 o, 431 p, 463 p
	h2	377 o, 431 p, 464 p
	c1	371, 378, 457
	c2	356, 456
$Ag_{0.7}Sb_{0.1}Sn_{0.2}$ (s.15)	h1	350 o, 506 p, 565 p, 600 p
	h2	311 o, 348, 506 o, 587 p, 603 p
	c1	362, 504, 514
	c2	362, 505, 518

60

J. Phase Equilib. Diffus. (2019) 40:53–63

Table 2 continued

Sample composition (sample no.)	Cycle (a)	Thermal signals Heating (b) and cooling (c) features, °C
Ag$_{0.595}$Sb$_{0.15}$Sn$_{0.255}$ (s.16)	h1	309 o, 355 o, 507 p, 544 p
	h2	232 o, 312 o, 354 o 507 p, 541 p
	c1	232, 365, 447
	c2	230, 359, 425
Ag$_{0.49}$Sb$_{0.3}$Sn$_{0.21}$ (s.17)	h1	376 o, 384 p, 414 p, 427 p, 450 p
	h2	377 o, 384 p, 424 p, 481 p
	c1	373, 385,
	c2	371, 382,
Ag$_{0.385}$Sb$_{0.45}$Sn$_{0.165}$ (s.18)	h1	376 o, 449, 479 p
	h2	376 o, 435 p, 448 p, 478 p
	c1	375, 410, 454
	c2	372, 383, 455
Ag$_{0.24}$Sb$_{0.2}$Sn$_{0.56}$ (s.19)	h1	233 o, 310, o, 335 p, 397 p
	h2	233 o, 310 o, 334 p, 405 p
	c1	232, 291, 317, 364
	c2	232, 291, 314, 377
Ag$_{0.225}$Sb$_{0.25}$Sn$_{0.525}$ (s.20)	h1	233 o, 310 o, 353 p, 401 p
	h2	233 o, 311 o, 352 p, 399 p
	c1	232, 294, 332, 355
	c2	232, 295, 335, 357
Ag$_{0.23}$Sb$_{0.25}$Sn$_{0.52}$ (s.21)	h1	233 o, 311 o, 338 p, 353 p, 398 p
	h2	233 o, 310 o, 337 p, 352 p, 399 p
	c1	232.5, 295, 332, 355
	c2	233, 295, 335, 357

Symbol meaning: o—onset, p—peak

(a) h1, h2 and c1, c2—from first and second heating and cooling curves, respectively

(b) Onset for invariant reactions, peak maximum otherwise

(c) From endset

Table 3 Heating and cooling features recorded during two temperature cycles with 1 °/min for sample of $X_{Ag}/X_{Sb} = 1$

Sample composition (sample no.)	Cycle (a)	Thermal signals Heating (b) and cooling (c) features, °C
Ag$_{0.1}$Sb$_{0.7}$Sn$_{0.2}$ (s. 1)	h1	377 o, 392 p, 538 p
	c1	355, 366, 514
Ag$_{0.1}$Sb$_{0.6}$Sn$_{0.3}$ (s.2)	h1	377 o, 382 p
	c1	374, 380
Ag$_{0.2}$Sb$_{0.2}$Sn$_{0.6}$ (s.5)	h1	234 o, 309 o, 328 p, 374 o, 386 p
	c1	233, 298, 313, 374
Ag$_{0.25}$Sb$_{0.25}$Sn$_{0.5}$ (s.7)	h1	234 o, 310 o, 330 p, 353 p, 421 p
	h2	234 o, 310 o, 330 p, 354 p, 423 p
	c1	232, 297, 333
	c2	232, 329, 297, 370

Symbol meaning: o—onset, p—peak

(a) h1, h2 and c1, c2—from first and second heating and cooling curves, respectively

(b) Onset for invariant reactions, peak maximum otherwise

(c) From endset

Table 4 Heating and cooling features recorded during two temperature cycles with 10 °/min

Sample composition (sample no.)	Cycle (a)	Thermal signals Heating (b) and cooling (c) features, °C
Ag$_{0.1}$Sb$_{0.7}$Sn$_{0.2}$ (s. 1)	h1	377 o, 538 p
	h2	377 o, 536 p
	c1	356, 366, 506
	c2	357, 366, 509
Ag$_{0.1}$Sb$_{0.6}$Sn$_{0.3}$ (s.2)	h1	366 o, 376 o, 489 p
	h2	366 o, 376 o, 490 p
	c1	356, 380, 466
	c2	357, 380, 476
Ag$_{0.2}$Sb$_{0.6}$Sn$_{0.2}$ (s.3)	h1	373 o, 420 p, 501 p
	h2	375 o, 420 p, 502 p
	c1	371, 492
	c2	374.6, 389, 493
Ag$_{0.2}$Sb$_{0.5}$Sn$_{0.3}$ (s.4)	h1	367 o, 453 p, 467 p
	h2	372 o, 455 p, 467 p
	c1	360, 444
	c2	359, 444
Ag$_{0.2}$Sb$_{0.2}$Sn$_{0.6}$ (s.5)	h1	233 o, 311 o, 334 p, 386 p
	c1	234, 289, 315, 370
Ag$_{0.25}$Sb$_{0.25}$Sn$_{0.5}$ (s.7)	h1	231 o, 312 o, 312 p, 359 p, 403 p
	c1	234, 291, 340, 348
Ag$_{0.65}$Sb$_{0.105}$Sn$_{0.245}$ (s.11)	h1	230.9 o, 311 o, 332 o, 503 o, 584 p
	h2	230.9 o, 311 o, 332 o, 503 o, 580.5 p
	c1	234, 290, 346, 474
	c2	234, 288, 350, 468

Symbol meaning: o—onset, p—peak

(a) h1, h2 and c1, c2—from first and second heating and cooling curves, respectively

(b) Onset for invariant reactions, peak maximum otherwise

(c) From endset

Table 5 Comparison of invariant reaction temperatures in Ag-Sb-Sn system obtained by experimental and assessment methods

Type of reaction	Invariant reactions	Temperature, °C						
		Ref 3 (a)	Ref 9 (b)	Ref 8 (a)	Ref 10 (b)	Ref 11 (b)	Ref 12 (a)	This work (a)
U$_1$	L + (Sb) ↔ ε + SbSn	378.5	375.0	379	388.1	379	375	376.5
P$_1$	L + ε + SbSn ↔ Sb$_2$Sn$_3$	…	328.9	…	…	…	…	…
U$_2$	L + Sb$_2$Sn$_3$ ↔ ε + β-Sn		231.6				…	…
U$_2$	L + SbSn ↔ ε + Sb$_2$Sn$_3$		…	314	311.2	313.5	308	309.9
U$_3$	L + Sb$_2$Sn$_3$ ↔ ε + β-Sn	234.8		233	231.4	231.5	229	231.8
P(?)	ε + SbSn + β-Sn ↔ Sb$_2$Sn$_3$	…	…	…		…	< 221	…

(a) Experimental

(b) Calculated

(samples 1-3, Table 6) or even third phase (sample 4, Table 6) in the ε phase matrix was observed.

In a sample 4 (Table 6) three phases were detected after equilibration, which form the equilibrium of (Sb) + ε + SbSn (Fig. 8b). Such three-phase field was suggested from results of experimental study of Lin et al.[6] (samples: 17-21). It should be underlined that the existence of three-phase equilibrium (Sb) + ε + SbSn in the Ag-Sb-Sn system was also suggested in the study of Masson and Kirkpatrick.[3]

62

J. Phase Equilib. Diffus. (2019) 40:53–63

The results obtained for sample 5 (Table 6) show the existence of two phase ε + SbSn equilibrium. This observation is compatible with the results of Lin et al.[6] who after annealing Ag-Sb-Sn samples at 400 °C detected such two-phase field between two three-phase equilibria
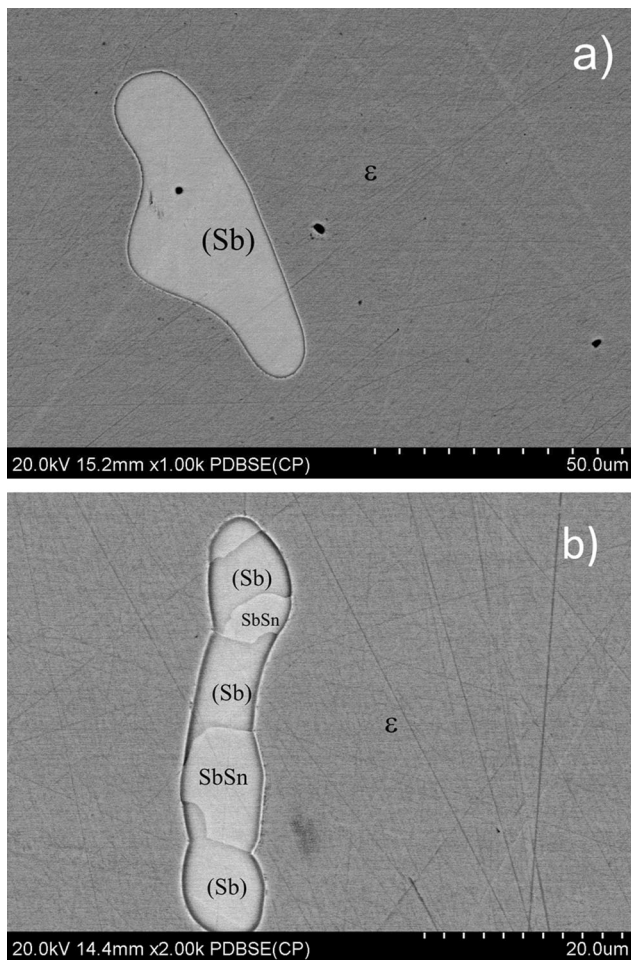

Fig. 8 BSE microphotographs of Ag-Sb-Sn samples equilibrated at 400 °C during 30 days. (a) Sample 0.74Ag-0.134Sb-0.126Sn, (b) Sample 0.74Ag-0.082Sb-0.178Sn. Black spots are holes

(Sb) + ε + SbSn and SbSn + ε + L, respectively. This topology does not agree with the ternary Ag-Sb-Sn diagram calculated at 400 °C from assessments of Oh et al.,[9] Moser et al.[10] and Gierlotka et al.,[11] in which other ternary equilibrium (Sb) + SbSn + L is present.

Again, it seems that the topological problems of the description of Sb-Sn rich part of this ternary system will be solved after the proper explanation of phase equilibria in the binary tin-antimony system.

In case of the equilibration experiments conducted at 300 °C the applied time was not long enough to reach the phase equilibrium in studied samples. The component concentrations in the phase grains in the same sample polished section differ from one another in such way that it was not possible to choose the proper one. So these results were rejected.

4 Conclusions

A topological data of the ternary Ag-Sb-Sn system has been measured, involving:

- the DTA study of phase transition temperatures by the analysis of 19 different samples in the temperature range 100-850 °C during the 1, 5 and 10 °/min heating and cooling cycles. The obtained results were compared with univariant and invariant temperatures calculated from available literature assessments of Ref 9-11 at the chosen phase diagram isopleth sections.
- the determination by SEM and EDX techniques of phase constituents and composition of coexisting phases of 5 samples after their thermal equilibration at 400 °C.

New results obtained in this work can improve the optimization process of the ternary Ag-Sb-Sn system. Especially, our own experimental results can be used in the verification of the temperatures of invariant reactions and

Table 6 Results of equilibration at 400 °C of samples of fixed initial composition

Sample no	Initial sample composition		Phases in equilibrium	Composition of phases after equilibration					
				Phase 1		Phase 2		Phase 3	
	x_{Ag}	x_{Sb}		x_{Ag}	x_{Sb}	x_{Ag}	x_{Sb}	x_{Ag}	x_{Sb}
1	0.740	0.134	(Sb) + ε	0.0	0.894	0.753	0.118	…	…
2	0.742	0.173	(Sb) + ε	0.0	0.904	0.750	0.171	…	…
3	0.720	0.063	(Sb) + ε	0.0	0.925	0.746	0.184	…	…
4	0.740	0.082	(Sb) + ε + SbSn	0.0	0.870	0.748	0.078	0.002	0.607
5	0.024	0.476	ε + SbSn	0.765	0.0	0.0	0.530	…	…

univariant lines (liquidus, solidus or solvus) of the Ag-Sb-Sn phase diagram.

References

1. H.T. Lee, M.H. Chen, H.M. Jao, and C.J. Hsu, Effect of Adding Sb on Microstructure and Adhesive Strength of Sn-Ag Solder Joints, *J. Electron. Mater.*, 2004, **33**, p 1048-1054, in English
2. H.T. Lee, H.S. Lin, C.S. Lee, and P.W. Chen, Reliability of Sn-Ag-Sb Lead-Free Solder Joints, *Mater. Sci. Eng. A*, 2005, **407**, p 36-44, in English
3. D.B. Masson and B.K. Kirkpatrick, Equilibrium Solidification Solder Alloys of Sn-Ag-Sb Thermal Fatigue-Resistant, *J. Electron. Mater.*, 1986, **15**(6), p 350-353, in English
4. P.J.T.L. Oberndorff, A.A. Kodentsov, V. Vuorinen, J.K. Kivilahti, and F.J.J. van Loo, Phase Relations in the Sn-Ag-Sb System at 220 °C, *Ber. Bunsenges. Phys. Chem.*, 1998, **102**(9), p 1321-1325, in English
5. R. Schmid-Fetzer, L. Rokhlin, E. Lysova, and M. Zinkevich, Silver-Antimony-Tin, Thermodynamic Properties Ternary Alloy Systems: Phase Diagrams, Crystallographic and Thermodynamic Data Critically Evaluated by MSIT, *Noble Metal Systems. Selected Systems from Ag-Al-Zn to Rh-Ru-Sc*, Vol 11B, G. Effenberg and S. Ilyenko, Ed., Springer, Berlin, 2006, p 181, in English
6. C.-Y. Lin, C. Lee, X. Liu, and Y.-W. Yen, Phase Equilibria of the Sn-Sb-Ag Ternary System and Interfacial Reactions at the Sn-Sb/Ag Joints at 400 °C and 150 °C, *Intermetallics*, 2008, **16**(2), p 230-238, in English
7. C. Lee, C.-Y. Lin, and Y.-W. Yen, The 260 °C Phase Equilibria of the Sn-Sb-Ag Ternary System and Interfacial Reactions at the Sn-Sb/Ag Joints, *J. Alloys Compd.*, 2008, **458**, p 436-445, in English
8. S.-W. Chen, P.-Y. Chen, C.-N. Chiu, Y.-C. Huang, and C.-H. Wang, Phase Equilibria of the Sn-Sb-Ag Ternary System (I): Experimental, *Metall. Mater. Trans. A*, 2008, **39A**(13), p 3191-3198, in English
9. C.S. Oh, J.H. Shim, B.J. Lee, and D.N. Lee, A thermodynamic study on the Ag-Sb-Sn system, *J. Alloys Compd.*, 1996, **238**, p 155-166, in English
10. Z. Moser, W. Gąsior, J. Pstruś, S. Ishihara, X.J. Liu, I. Ohnuma, R. Kainuma, and K. Ishida, Surface Tension and Density Measurements of Sn-Ag-Sb Liquid Alloys and Phase Diagram Calculations of the Sn-Ag-Sb ternary system, *Mater. Trans.*, 2004, **45**(3), p 652-660, in English
11. W. Gierlotka, Y.-C. Huang, and S.-W. Chen, Phase Equilibria of Sn-Sb-Ag Ternary System (II): Calculation, *Metall. Mater. Trans. A*, 2008, **39**(13), p 3199-3209, in English
12. D. Li, S. Delsante, A. Watson, and G. Borzone, The Effect of Sb Addition on Sn-Based Alloys for High-Temperature Lead-Free Solders: An Investigation of the Ag-Sb-Sn System, *J. Electron. Mater.*, 2012, **4**(1), p 67-85, in English
13. C. Schmetterer, J. Polt, and H. Flandorfer, The Phase Equilibria in the Sb-Sn System—Part II: Experimental Results, *J. Alloys Compd.*, 2018, **743**(4), p 523-536, in English
14. J. Łapsa and B. Onderka, Thermodynamic Properties of Liquid Silver-Antimony-Tin Alloys Determined from Electrochemical and Calorimetric Measurements, *J. Electron. Mater.*, 2016, **45**(8), p 4441-4452, in English
15. B. Gather, P. Schröter, and R. Blachnik, Mixing Enthalpy of Ternary Systems Ag-In-Sn, Ag-Sn-Sb, Ag-In-Sb and In-Pb-Sb, *Z. Metallkde.*, 1987, **78**(4), p 280-285, in English
16. W.J. Boettinger, U.R. Kattner, K.-W. Moon, and J. Perepezko, *DTA and Heat-flux DSC Measurements of Alloy Melting and Freezing*, NIST Special Publication 960-15, 2006, in English